Available online at www.sciencedirect.com
SCIENCE DIRECT
Journal of Magnetic Resonance 181 (2006) 296–303
JMR Journal of Magnetic Resonance
www.elsevier.com/locate/jmr

Finite pulse width artifact suppression in spin-1 quadrupolar echo spectra by phase cycling

E.S. Mananga, Y.S. Rumala, G.S. Boutis *

York College, The City University of New York, Department of Natural Sciences, Physics, 94-20 Guy R. Brewer Blvd., Jamaica, NY 11451, USA

Received 31 March 2006; revised 18 May 2006
Available online 19 June 2006

Abstract

A phase cycling scheme for suppressing spectral artifacts introduced in quadrupolar echo spectroscopy of spin-1 nuclei due to finite pulse width effects is presented. The phase cycling scheme is developed using the formalism of average Hamiltonian theory and fictitious spin-1 operators. A simulation and experiment on deuterated polyethelene is performed highlighting the spectral artifact introduced by finite pulse widths and successful removal with the proposed phase cycling scheme.

Keywords: Quadrupolar echo; Finite pulse widths; Deuterium NMR; Phase cycling; Average Hamiltonian theory

1. Introduction

An experimentally challenging aspect of solid state nuclear magnetic resonance is the requirement of delivering a strong radio frequency (RF) pulse to modulate the nuclear spins in the presence of a dipolar or quadrupolar interaction. Quite often, if the pulse power is substantial, one can ignore the spin system's evolution during the RF pulses and approximate them as ideal δ-function perturbations. However, there are a multitude of NMR experiments where this approximation is not valid, and accounting for finite pulse width effects can drastically improve upon a cycles' performance. For example, the celebrated WAHUHA cycle as well as many other multiple pulse sequences were significantly improved upon when finite pulse widths were properly accounted for [1].

In this work, we investigate the finite pulse width artifacts introduced in spin-1 quadrupolar echo spectroscopy. To suppress the artifacts introduced from the ring down of the RF coil, a spin echo is applied in this technique for studying the broad quadrupolar spectra of a solid spin system. The method involves acquiring the peak of an echo, which under ideal experimental conditions and no relaxation, would yield a signal precisely equal to that of the free induction decay of a single pulse [2]. This scheme has been applied with great success for understanding various properties such as the orientation and rate of rotation of molecules of a broad range of polymer [3,4], solid [5] and semisolid [6] systems.

The signal acquired by a spin echo, however, is never free of instrumental artifacts often making interpretation of data challenging. A variety of techniques have been introduced to alleviate distortions commonly encountered in echo spectroscopy of spin-1 nuclei including phase cycling schemes for suppressing pulse transients and imperfect $\pi/2$ pulses [7], co-adding spectra acquired with different pulse spacings, or adding a two-dimensional Fourier transform for removing feed-through signals [8] and using composite pulses or chirped pulses for alleviating pulse power issues [9–13]. An additional artifact often encountered causes an asymmetry of the spectra due to the evolution of the spin system under the quadrupolar Hamiltonian *during* the RF pulses.

Previous work associated with spectral artifacts due to finite pulse widths in a two pulse echo experiment have been reported and described in detail by Bloom et al.

* Corresponding author. Fax: +1 718 262 2652.
E-mail address: gboutis@york.cuny.edu (G.S. Boutis).

1090-7807/$ - see front matter © 2006 Elsevier Inc. All rights reserved.
doi:10.1016/j.jmr.2006.05.015

[14] and Henrichs et al. [15]. Their work showed that one can remove distortions due to finite pulse widths by scaling the experimental data by a multiplicative factor determined a priori. In this paper we describe how the spectra of spin-1 nuclei are distorted due to finite pulse widths in a two-pulse echo experiment, and how one can suppress these artifacts to first-order by cycling the phases of both the receiver and transmitter. The approach makes use of the spin-1 operator formalism developed by Vega and Pines [16] together with average Hamiltonian theory developed by Waugh and co-workers [17]. Our results are verified using a home-written simulation program and tested experimentally on a sample of deuterated polyethelene.

2. Theory

In the following, we analyze the spin dynamics of spin-1 nuclei evolving under the first-order secular quadrupolar interaction subject to a large, static and homogeneous field and the two pulse RF sequence shown in Fig. 1. We assume that the quadrupolar interaction is significantly larger than any heteronuclear and homonuclear dipole interactions as well as any resonance offset present and that the system of interest is non-metallic, so that any paramagnetic shift anisotropy can be ignored. The cycle shown in the figure is known to refocus the time evolution of spin-1 nuclei evolving under the first-order secular quadrupolar interaction which is given by

$$H_{\omega_Q} = \omega'_Q R_{2,0} \frac{1}{\sqrt{6}} [12 I_{z,1} I_{z,1} - II] \tag{1}$$

In the above expression $R_{2,0} = \sqrt{\frac{3}{2}}[P_2(\cos(\theta)) + (\frac{\eta}{2})\cos(2\theta)\sin^2(\varphi)]$, $P_2(\cos(\theta))$ is the second-order Legendre polynomial of $\cos(\theta)$, θ and φ are two of the three Euler angles and $\omega'_Q = \frac{e^2 qQ}{2I(2I-1)\hbar}$ [18]. The Hamiltonian has been written using the spin-1 operator formalism of Vega and Pines [16] where the spin operators are

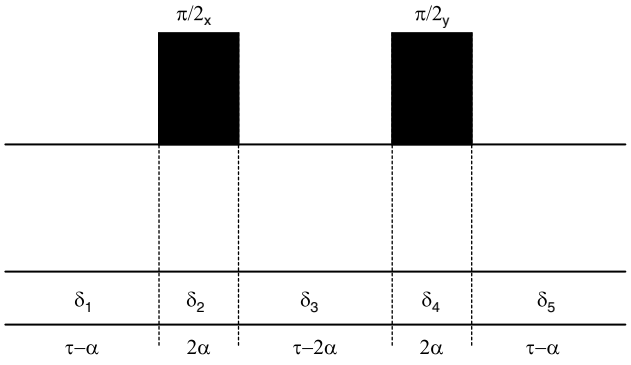

Fig. 1. Two pulse sequence for refocusing the quadrupolar Hamiltonian. In the figure, the two π/2 pulses have a width of 2α and the phases of the two pulses shown as x and y can be any combination of 90 degree phase shifted pulses.

$$I_{p,1} = \tfrac{1}{2} I_p \tag{2}$$

$$I_{p,2} = \tfrac{1}{2}(I_q I_r + I_r I_q) \tag{3}$$

$$I_{p,3} = \tfrac{1}{2}(I_r^2 - I_q^2) \tag{4}$$

with $p = x,\ y,\ z$ and $(p,q,r) = (x,y,z)$ with cyclic permutations [16]. An illuminating approach for studying the dynamics of a spin system subject to an RF perturbation, given by Waugh and co-workers [17], is to consider the average or effective Hamiltonian of the RF pulse train. This approach will be shown to provide insight into how the finite pulse widths affect the system evolution. In this formalism, the time evolution of the system from time $t = 0$, $\rho(0)$ to the state at time $t = t_c$, $\rho(t_c)$ is given by

$$\rho(t_c) = U_{\mathrm{RF}} U_{\mathrm{int}} \rho(0) U_{\mathrm{int}}^{-1} U_{\mathrm{RF}}^{-1} \tag{5}$$

where the propagator U_{RF} is given by the Dyson series

$$U_{\mathrm{RF}} = \ldots U_3 U_2 U_1 U_0 \tag{6}$$

and U_{int} is given by the Magnus expansion

$$U_{\mathrm{int}}(t,0) = \exp[-\mathrm{i}t_c(\overline{H}^0_{\mathrm{int}} + \overline{H}^1_{\mathrm{int}} + \cdots)] \tag{7}$$

with

$$\overline{H}^0_{\mathrm{int}} = \frac{1}{t_c}\int_0^{t_c} \widetilde{H}_{\mathrm{int}}(\tau)\mathrm{d}t \tag{8}$$

$$\overline{H}^1_{\mathrm{int}} = \frac{-\mathrm{i}}{2t_c}\int_0^{t_c} [\widetilde{H}_{\mathrm{int}}(\tau), \int_0^{\tau} \widetilde{H}_{\mathrm{int}}(\phi)\mathrm{d}\phi]\mathrm{d}\tau \tag{9}$$

$$\overline{H}^2_{\mathrm{int}} = \ldots \tag{10}$$

In the above, U_{RF} represents the interaction associated with the sequence of RF pulses applied over a time t_c, and H_{int} refers to the systems' internal Hamiltonian. An attractive feature of average Hamiltonian theory is that a variety of Hamiltonians can be accounted for in the system evolution including pulse errors and finite pulse width effects.

For conciseness we rewrote the quadrupolar Hamiltonian given in Eq. (1) more compactly as

$$H_{\omega_Q} = \omega_Q [12 I_{z,1} I_{z,1} - II] \tag{11}$$

where $\omega_Q = \omega'_Q R_{2,0}\frac{1}{\sqrt{6}}$, and take the initial state of the system to be given by $\rho(0) = I_{z,1}$.

To calculate the resulting zeroth-order term of the quadrupolar Hamiltonian in the Magnus expansion, we constructed Table 1 and computed the toggling frame quadrupolar Hamiltonian, $\widetilde{H}_{\omega_Q}$, during each stage of the pulse cycle. Referring to Fig. 1, for the first time interval $0 \leqslant t < \tau - \alpha$, $U_{\mathrm{RF}} = 1$. For the second interval $\tau - \alpha \leqslant t \leqslant \tau + \alpha$, the rotation is given by the linear parametrization:

$$\theta(t) = \frac{\pi}{4}\left[1 + \frac{t-\tau}{\alpha}\right] \tag{12}$$

with $\theta = 0$ at $t = \tau - \alpha$, and $\theta = \frac{\pi}{2}$ at $t = \tau + \alpha$. For the fourth interval $2\tau - \alpha \leqslant t \leqslant 2\tau + \alpha$, the transformation for the RF pulse is given by

Table 1
Transformations of the operator U_{RF} and the toggling frame quadrupolar Hamiltonian during each stage of the quadrupolar echo sequence shown in Fig. 1

Interval	Time	U_{RF}	$\widetilde{H_{\omega_Q}}$
δ_1	$0 \leqslant t \leqslant \tau - \alpha$	1	$\omega_Q[12I_{z,1}I_{z,1} - II]$
δ_2	$\tau - \alpha \leqslant t \leqslant \tau + \alpha$	$\exp[2i\theta(t)I_{x,1}]$	$\omega_Q[12I_{z,1}\ I_{z,1}\cos^2(\theta) + 12I_{y,1}\ I_{y,1}\ \sin^2(\theta) + \ 6I_{x,2}\sin(\theta)\cos(\theta) - II]$
δ_3	$\tau + \alpha \leqslant t \leqslant 2\tau - \alpha$	$\exp[i\pi I_{x,1}]$	$\omega_Q[12I_{y,1}\ I_{y,1} - II]$
δ_4	$2\tau - \alpha \leqslant t \leqslant 2\tau + \alpha$	$\exp[2i\theta(t)I_{y,1}]\times\exp[i\pi I_{x,1}]$	$\omega_Q[12I_{y,1}I_{y,1}\cos^2(\theta) + 12I_{x,1}I_{x,1}\sin^2(\theta) - 6I_{z,2}\sin(\theta)\cos(\theta) - II]$
δ_5	$2\tau + \alpha \leqslant t \leqslant 3\tau$	$\exp[i\pi I_{y,1}]\times\exp[i\pi I_{x,1}]$	$\omega_Q[12I_{x,1}\ I_{x,1} - II]$

$\omega_Q = \omega'_Q R_{2,0}\frac{1}{\sqrt{6}}$ and $\omega'_Q = \frac{e^2qQ}{2I(2I-1)\hbar}$.

$$\theta(t) = \frac{\pi}{4}\left[1 + \frac{t-2\tau}{\alpha}\right] \tag{13}$$

with $\theta = 0$ at $t = 2\tau - \alpha$ and $\theta = \frac{\pi}{2}$ at $t = 2\tau + \alpha$. Table 1 gives the toggling frame Hamiltonians during each stage of the evolution that were developed knowing the transformations of $I_{x,1}$, $I_{y,1}$ and $I_{z,1}$. The resulting toggling frame Hamiltonians were integrated over their respective time intervals and are given in Table 2. The zeroth-order terms of the Magnus expansion were calculated for all possible eight cycles that can refocus the spin magnetization and produce an echo.

Consider the case of a $\pi/2$ pulse about the x-axis followed by a $\pi/2$ pulse about the y-axis. From Table 2, the zeroth-order term of the Magnus expansion is given by

$$\overline{H}^0_{\omega_Q} = \frac{4\alpha\omega_Q}{\pi\tau}[I_{x,2} - I_{z,2}] \tag{14}$$

Two important findings of this result should be recognized. First, when $\alpha = 0$ the zeroth-order term vanishes. In this situation, the density matrix at $t = 3\tau$, calculated using Eq. (5), is found to be $\rho_{x,y}(3\tau) = I_{y,1}$, corresponding to the case of perfect refocusing of the spin magnetization with no additional quantum coherences present to first-order of the Magnus expansion. This is what one would expect in the case of δ-function RF pulses. Second, the result indicates that the contribution of finite pulse widths to the system evolution becomes less important for large values τ. In practice the efficiency of refocusing the spin dynamics of dipolar or quadrupolar coupled spins with this two pulse cycle is known from multiple pulse NMR to decrease with large pulse spacings, making the use of large spacings between pulses impractical [17]. In order to remove the contribution of finite pulse widths in the system evolution we consider Eqs. (5) and (14) and determine the state of the spin system at 3τ and the detected signal.

Table 2
Integrated first-order terms of the Magnus expansion for the quadrupolar Hamiltonian for eight cycles of the quadrupolar echo pulse sequence in Fig. 1 that produce an echo

Pulse 1	Pulse 2	$\overline{H}^0_{\omega_Q}$
x	y	$\frac{w}{3\tau}[I_{x,2} - I_{z,2}]$
x	$-y$	$\frac{w}{3\tau}[I_{x,2} + I_{z,2}]$
$-x$	y	$\frac{w}{3\tau}[-I_{x,2} + I_{z,2}]$
$-x$	$-y$	$\frac{w}{3\tau}[-I_{x,2} - I_{z,2}]$
y	x	$\frac{w}{3\tau}[-I_{z,2} - I_{y,2}]$
y	$-x$	$\frac{w}{3\tau}[I_{z,2} - I_{y,2}]$
$-y$	x	$\frac{w}{3\tau}[I_{z,2} + I_{y,2}]$
$-y$	$-x$	$\frac{w}{3\tau}[-I_{z,2} + I_{y,2}]$

$w = \frac{12\alpha\omega_Q}{\pi}$, where ω_Q is the quadrupolar coupling constant and 2α is the $\pi/2$ pulse width.

After a lengthy calculation, the density matrix at 3τ for a $\pi/2$ pulse about the x-axis followed by a $\pi/2$ pulse about the y-axis is found to be

$$\begin{aligned}\rho_{x,y}(3\tau) =& \frac{\sin(\sqrt{2}w)}{\sqrt{2}}I_{x,2} \\ &+ \frac{1}{2}\left[\cos\left(\frac{w}{\sqrt{2}}\right) + \cos(w\sqrt{2})\right]I_{y,1} \\ &- \frac{1}{2}\left[\cos\left(\frac{w}{\sqrt{2}}\right) - \cos(w\sqrt{2})\right]I_{z,1} + \frac{\sin(\sqrt{2}w)}{\sqrt{2}}I_{y,3} \\ &+ \frac{1}{4}\left[-2\sqrt{2}\sin\left(\frac{w}{\sqrt{2}}\right) + \sqrt{2}\sin(w\sqrt{2})\right]I_{x,3}\end{aligned} \tag{15}$$

where $w = \frac{12\alpha\omega_Q}{\pi}$. When α=0 the result above reduces to $\rho_{x,y}(3\tau) = I_{y,1}$, which is indeed what one would expect in the situation of δ-function RF pulses. The terms $I_{x,3}$ and $I_{y,3}$ commute with the quadrupolar interaction and consequently do not evolve and are not detectable. However, $I_{x,2}$ does not commute with the quadrupolar Hamiltonian and evolves to a detectable signal which produces a spectral distortion as we will now show Using the Liouville–Von Neumann equation, the quadrupolar Hamiltonian in Eq. (11) and $\rho_{x,y}(3\tau)$ the density matrix at a time $t + 3\tau$ is found to be

$$\begin{aligned}\rho_{x,y}(t+3\tau) =& \frac{1}{\sqrt{2}}\cos\left(\frac{2}{3}\omega_Q t\right)\sin(w\sqrt{2})I_{x,2} \\ &+ \frac{1}{2}\cos(\omega_Q t)\left[\cos\left(\frac{w}{\sqrt{2}}\right) + \cos\left(w\sqrt{2}\right)\right]I_{y,1} \\ &- \frac{1}{2}\cos\left(\frac{1}{3}\omega_Q t\right)\left[\cos\left(\frac{w}{\sqrt{2}}\right) - \cos\left(w\sqrt{2}\right)\right]I_{z,1} \\ &+ \frac{\sin(\sqrt{2}w)}{\sqrt{2}}I_{y,3}\frac{1}{4}\left[-2\sqrt{2}\sin\left(\frac{w}{\sqrt{2}}\right) + \sqrt{2}\sin(w\sqrt{2})\right]I_{x,3} \\ &- \frac{1}{2}\sin(\omega_Q t)\left[\cos\left(\frac{w}{\sqrt{2}}\right) + \cos(w\sqrt{2})\right]I_{y,2} \\ &- \frac{1}{2}\sin\left(\frac{1}{3}\omega_Q t\right)\left[\cos\left(\frac{w}{\sqrt{2}}\right) - \cos(w\sqrt{2})\right]I_{z,2} \\ &- \frac{1}{\sqrt{2}}\sin\left(\frac{2}{3}\omega_Q t\right)\sin(\sqrt{2}w)I_{x,1}\end{aligned} \tag{16}$$

The signal detected as a function of time is formally given by $\text{Signal}(t+3\tau) = \text{Trace}((I_{x,1} + \mathrm{i}I_{y,1})\rho(3\tau + t))$ which reduces to

$$\text{Signal}_{x,y}(t+3\tau) = \mathrm{i}\left(\frac{1}{2}\cos(\omega_Q t)\left[\cos\left(\frac{w}{\sqrt{2}}\right) + \cos(w\sqrt{2})\right]\right) - \left(\frac{1}{\sqrt{2}}\sin\left(\frac{2}{3}\omega_Q t\right)\sin(\sqrt{2}w)\right) \quad (17)$$

In the above expression for $\rho_{x,y}(t+3\tau)$, the term $\sin(\frac{2}{3}\omega_Q t)\sin(\sqrt{2}w)$ multiplying $I_{x,1}$ arises from the time evolution of the term $I_{x,2}$ in $\rho_{x,y}(3\tau)$ and is an odd function. It indeed vanishes in the case of delta function RF pulses ($\alpha = 0, w = \frac{12\alpha\omega_Q}{\pi} = 0$). However, the term multiplying $I_{y,1}$ in $\rho_{x,y}(t+3\tau)$, $\frac{1}{2}\cos(\omega_Q t)[\cos(w/\sqrt{2}) + \cos(\sqrt{2}w)]$, is an even function and is the desired signal. As a consequence, the combination of the odd and even functions results in a slightly asymmetric spectrum causing one of the peaks of the quadrupolar powder pattern to be slightly higher than the other.

The density matrices at 3τ for all eight possible combinations of phase shifted RF pulses are provided in Table 3 with each highlighting the effect of finite pulse widths on the system evolution and the state of the system at 3τ. Referring to Table 3, all $\pm x$, $\pm y$ cycles create a term $I_{x,2}$ and all $\pm y$, $\pm x$ cycles create a term $I_{y,2}$ due to finite pulse widths. These terms evolve to detectable coherence $I_{x,1}$ and $I_{y,1}$, respectively, and result in a spectral distortion as described above for the x, y cycle.

With the goal of canceling the contribution of finite pulse width artifacts in the detected signal, we wish to remove the terms $I_{x,2}$ and $I_{y,2}$ in the density matrix at 3τ. Referring to Table 3, one such phase cycle is the addition of an x, y cycle with an x, $-y$ cycle acquired with identical receiver phases. Another possible combination of pulse cycles that suppresses finite pulse widths, which is also robust against other artifacts, is given by the following phase cycling scheme

$$\begin{aligned}\phi_1 &= \{x, x, -x, -x, y, y, -y, -y\}\\ \phi_2 &= \{y, -y, y, -y, x, -x, x, -x\}\\ RP &= \{270, 270, 90, 90, 0, 0, 180, 180\}\end{aligned} \quad (18)$$

where ϕ_1 is the phase of the first pulse, ϕ_2 is the phase of the second pulse and RP is the receiver phase and is given in degrees. The above phase cycling scheme is found to be independent of α and the finite pulse width contribution to the signal detected is removed. This can be shown by using the results in Table 3 and performing the calculation for the signal detected, which is formally given by the following calculation

$$\begin{aligned}\text{Signal}(3\tau) = \text{Trace}\{&(\rho_{x,y}(3\tau) + \rho_{x,-y}(3\tau)\\ &- \rho_{-x,y}(3\tau) - \rho_{-x,-y}(3\tau))(-I_{y,1} + \mathrm{i}I_{x,1})\\ &+ (\rho_{y,x}(3\tau) + \rho_{y,-x}(3\tau)\\ &- \rho_{-y,x}(3\tau) - \rho_{-y,-x}(3\tau))(I_{x,1} + \mathrm{i}I_{y,1})\}\end{aligned} \quad (19)$$

By using the density matrices in Table 3, the above expression reduces to

$$\begin{aligned}\text{Signal}(3\tau) = 4&\left(\cos\left(\frac{w}{\sqrt{2}}\right) + \cos(w\sqrt{2})\right)\\ &\times \text{Trace}\{-I_{y,1}(-I_{y,1} + \mathrm{i}I_{x,1}) + I_{x,1}(I_{x,1} + \mathrm{i}I_{y,1})\}\end{aligned} \quad (20)$$

which has no dependence on $I_{x,2}$ or $I_{y,2}$ in the argument of the Trace operator that were shown to cause a spectral asymmetry. The modulation $4(\cos(\frac{w}{\sqrt{2}}) + \cos(w\sqrt{2}))$, however, results in a small reduction in signal amplitude due to finite pulse widths. This phase cycling scheme is indeed based on the familiar CYCLically Ordered Phase Sequence(CYCLOPS) developed by Hoult and Richards [19], already known in the NMR community to suppress the ringdown effects of the second pulse and remove imbalances in the channels of the receiver. This phase cycling scheme also suppresses the free induction decay from the second pulse that may distort the signal detected when perfect $\pi/2$ pulses are not delivered to the spin system. While our calculations assumed perfect $\pi/2$ pulses, this requirement

Table 3
Density matrices at 3τ, $\rho(3\tau)$, for eight cycles of the quadrupolar echo pulse sequence for a system evolving under the first-order secular quadrupolar Hamiltonian

Pulse 1	Pulse 2	$\rho(3\tau)$
x	y	$\frac{\sin(\sqrt{2}w)}{\sqrt{2}}I_{x,2} + \frac{1}{2}[\cos(\frac{w}{\sqrt{2}}) + \cos(w\sqrt{2})]I_{y,1} - \frac{1}{2}[\cos(\frac{w}{\sqrt{2}}) - \cos(w\sqrt{2})]I_{z,1} + \frac{\sin(\sqrt{2}w)}{\sqrt{2}}I_{y,3} + \frac{1}{4}[-2\sqrt{2}\sin(\frac{w}{\sqrt{2}}) + \sqrt{2}\sin(w\sqrt{2})]I_{x,3}$
x	$-y$	$-\frac{\sin(\sqrt{2}w)}{\sqrt{2}}I_{x,2} + \frac{1}{2}[\cos(\frac{w}{\sqrt{2}}) + \cos(w\sqrt{2})]I_{y,1} - \frac{1}{2}[\cos(\frac{w}{\sqrt{2}}) - \cos(w\sqrt{2})]I_{z,1} - \frac{\sin(\sqrt{2}w)}{\sqrt{2}}I_{y,3} - \frac{1}{4}[-2\sqrt{2}\sin(\frac{w}{\sqrt{2}}) + \sqrt{2}\sin(w\sqrt{2})]I_{x,3}$
$-x$	y	$\frac{\sin(\sqrt{2}w)}{\sqrt{2}}I_{x,2} - \frac{1}{2}[\cos(\frac{w}{\sqrt{2}}) + \cos(w\sqrt{2})]I_{y,1} - \frac{1}{2}[\cos(\frac{w}{\sqrt{2}}) - \cos(w\sqrt{2})]I_{z,1} - \frac{\sin(\sqrt{2}w)}{\sqrt{2}}I_{y,3} - \frac{1}{4}[-2\sqrt{2}\sin(\frac{w}{\sqrt{2}}) + \sqrt{2}\sin(w\sqrt{2})]I_{x,3}$
$-x$	$-y$	$-\frac{\sin(\sqrt{2}w)}{\sqrt{2}}I_{x,2} - \frac{1}{2}[\cos(\frac{w}{\sqrt{2}}) + \cos(w\sqrt{2})]I_{y,1} - \frac{1}{2}[\cos(\frac{w}{\sqrt{2}}) - \cos(w\sqrt{2})]I_{z,1} + \frac{\sin(\sqrt{2}w)}{\sqrt{2}}I_{y,3} + \frac{1}{4}[-2\sqrt{2}\sin(\frac{w}{\sqrt{2}}) + \sqrt{2}\sin(w\sqrt{2})]I_{x,3}$
y	x	$-\frac{\sin(w/\sqrt{2})}{\sqrt{2}}I_{y,3} - \frac{\sin(\sqrt{2}w)}{2\sqrt{2}}I_{z,3} + \frac{\sin(\sqrt{2}w)}{2\sqrt{2}}I_{x,3} + \frac{1}{2}[\cos(w\sqrt{2}) - \cos(w/\sqrt{2})]I_{z,1} + \frac{\sin(\sqrt{2}w)}{2\sqrt{2}}I_{y,2} - \frac{1}{2}[\cos(w\sqrt{2}) + \cos(w/\sqrt{2})]I_{x,1}$
y	$-x$	$\frac{\sin(w/\sqrt{2})}{\sqrt{2}}I_{y,3} + \frac{\sin(\sqrt{2}w)}{2\sqrt{2}}I_{z,3} - \frac{\sin(\sqrt{2}w)}{2\sqrt{2}}I_{x,3} + \frac{1}{2}[\cos(w\sqrt{2}) - \cos(w/\sqrt{2})]I_{z,1} - \frac{\sin(\sqrt{2}w)}{2\sqrt{2}}I_{y,2} - \frac{1}{2}[\cos(\sqrt{2}w) + \cos(w/\sqrt{2})]I_{x,1}$
$-y$	x	$\frac{\sin(w/\sqrt{2})}{\sqrt{2}}I_{y,3} + \frac{\sin(\sqrt{2}w)}{2\sqrt{2}}I_{z,3} - \frac{\sin(\sqrt{2}w)}{2\sqrt{2}}I_{x,3} + \frac{1}{2}[\cos(w\sqrt{2}) - \cos(w/\sqrt{2})]I_{z,1} + \frac{\sin(\sqrt{2}w)}{2\sqrt{2}}I_{y,2} + \frac{1}{2}[\cos(\sqrt{2}w) + \cos(w/\sqrt{2})]I_{x,1}$
$-y$	$-x$	$-\frac{\sin(w/\sqrt{2})}{\sqrt{2}}I_{y,3} - \frac{\sin(\sqrt{2}w)}{2\sqrt{2}}I_{z,3} + \frac{\sin(\sqrt{2}w)}{2\sqrt{2}}I_{x,3} + \frac{1}{2}[\cos(w\sqrt{2}) - \cos(w/\sqrt{2})]I_{z,1} - \frac{\sin(\sqrt{2}w)}{2\sqrt{2}}I_{y,2} + \frac{1}{2}[\cos(\sqrt{2}w) + \cos(w/\sqrt{2})]I_{x,1}$

$w = \frac{12\alpha\omega_Q}{\pi}$, ω_Q is the quadrupolar coupling constant, 2α is the $\pi/2$ pulse width and we have set $\frac{\gamma\hbar B_o}{kT} = 1$.

is never achievable in NMR experiments and produces quantum coherences that distort the spectra of spin-1 nuclei. Antonijevic and Wimperis [20] have recently described phase cycling schemes for coherence pathway selection in quadrupolar echo experiments that are robust in suppressing such distortions. Their work showed that the creation of quantum coherence in the two pulse cycle shown in Fig. 1 due to field inhomogeneity and pulse imperfections can be removed by the same cycle suggested in Eq. (18). In addition to the eight step cycle, they suggested more complex phase cycling schemes for refocusing both offset and quadrupolar interactions, which is not the subject of the work presented.

Furo and Hedin [7] have also reported on a novel phase cycling scheme that removes ringdown effects for the same two pulse echo sequence analyzed here. Their work shows how to cancel the electronic ringing signal that is phase coherent with the first pulse, and is not affected by the second pulse but distorts the detected signal when the spacing between pulses is short. Their phase cycling scheme is

$$\begin{aligned}\phi_1 &= \{x\}\\ \phi_2 &= \{x,y,-x,-y\}\\ RP &= \{270,90,270,90\}\end{aligned} \tag{21}$$

For the purposes of also removing finite pulse width artifacts in addition to canceling such ringdown effects, we calculated the first-order term of the Magnus expansion for the cycles $\phi_1 = x$ with $\phi_2 = x, -x$, and other possible similar combinations. The resulting zeroth-order terms of the Magnus expansion for these cycles are given in Table 4, and the density matrices at 3τ are given in Table 5. Considering the result in Table 5 with that in Table 3, we find that the phase cycling scheme above does not suppress finite pulse width contributions to the signal even though it is robust against ringdown effects. In their work, Furo and Hedin suggest more complex phase cycling schemes that involve cycling the phases of all the pulses and the receiver as follows

$$\begin{aligned}\phi_1 &= \{x,x,x,x,-x,-x,-x,-x,y,y,y,y,-y,-y,-y,-y\}\\ \phi_2 &= \{x,y,-x,-y,y,x,-y,-x,y,x,-y,-x,x,y,-x,-y\}\\ RP &= \{90,270,90,270,90,270,90,270,180,0,180,0,\\ &\quad 180,0,180,0\}\end{aligned} \tag{22}$$

Using Tables 3 and 5, the corresponding density matrix when all the cycles are added and subtracted as indicated for the above phase cycle at 3τ is

$$\begin{aligned}\rho(3\tau) = 2\Bigg[&-\cos\left(\frac{\omega}{\sqrt{2}}\right)-\cos(\sqrt{2}\omega)\\ &+\frac{8\alpha}{\pi}\sin\left(\frac{3w_1}{4}\right)\frac{\sinh\left(\frac{3\omega_Q}{2}\sqrt{-\left(\tau^2+\frac{\alpha^2}{\pi^2}\right)}\right)}{\sqrt{-\left(\tau^2+\frac{\alpha^2}{\pi^2}\right)}}\Bigg]I_{y,1}\\ &+2\Bigg[-\cos\left(\frac{\omega}{\sqrt{2}}\right)-\cos(\sqrt{2}\omega)\\ &+\frac{8\alpha}{\pi}\sin\left(\frac{3w_1}{4}\right)\frac{\sinh\left(\frac{3\omega_Q}{2}\sqrt{-\left(\tau^2+\frac{\alpha^2}{\pi^2}\right)}\right)}{6\omega_Q\sqrt{-\left(\tau^2+\frac{\alpha^2}{\pi^2}\right)}}\Bigg]I_{x,1}\\ &-\frac{16\alpha}{\pi}\cos\left(\frac{3w_1}{4}\right)\frac{\sinh\left(\frac{3\omega_Q}{2}\sqrt{-\left(\tau^2+\frac{\alpha^2}{\pi^2}\right)}\right)}{\sqrt{-\left(\tau^2+\frac{\alpha^2}{\pi^2}\right)}}I_{x,2}\\ &+\frac{16\alpha}{\pi}\cos\left(\frac{3w_1}{4}\right)\frac{\sinh\left(\frac{3\omega_Q}{2}\sqrt{-\left(\tau^2+\frac{\alpha^2}{\pi^2}\right)}\right)}{\sqrt{-\left(\tau^2+\frac{\alpha^2}{\pi^2}\right)}}I_{y,2}\end{aligned} \tag{23}$$

Table 4
Integrated first-order terms of the Magnus expansion for the quadrupolar Hamiltonian for all eight cycles suggested by Furo and Hedin [7] useful for suppressing ringdown effects in quadrupolar echo experiments

Pulse 1	Pulse 2	$\overline{H}^0_{\omega_Q}$
x	x	$-2\omega_Q I_{y,3}$
x	$-x$	$2\omega_Q I_{y,3} - \frac{8\alpha\omega_Q}{\pi\tau} I_{x,2}$
$-x$	x	$2\omega_Q I_{y,3} + \frac{8\alpha\omega_Q}{\pi\tau} I_{x,2}$
$-x$	$-x$	$-2\omega_Q I_{y,3}$
y	y	$2\omega_Q I_{x,3}$
y	$-y$	$-2\omega_Q I_{y,3} + \frac{8\alpha\omega_Q}{\pi\tau} I_{y,2}$
$-y$	y	$-2\omega_Q I_{y,3} - \frac{8\alpha\omega_Q}{\pi\tau} I_{y,2}$
$-y$	$-y$	$2\omega_Q I_{x,3}$

ω_Q is the quadrupolar coupling constant and 2α is the $\pi/2$ pulse width.

Table 5
Density matrices at 3τ, $\rho(3\tau)$, for the eight cycles suggested by Furo and Hedin [7] for suppressing ringdown artifacts of the RF coil

Pulse 1	Pulse 2	$\rho(3\tau)$
x	x	$-\cos(3\tau\omega_Q)I_{z,1} - \sin(3\tau\omega_Q)I_{z,2}$
x	$-x$	$+\frac{48\alpha\omega_Q}{\pi} S_1 \sin(\frac{9\tau\omega_Q}{2}) I_{y,1} + \frac{48\alpha\omega_Q}{\pi} S_1 \cos(\frac{9\tau\omega_Q}{2}) I_{y,2} + [C_1 \cos(\frac{9\tau\omega_Q}{2}) + 6\tau\omega_Q S_1 \sin(\frac{9\tau\omega_Q}{2})] I_{z,1} + [C_1 \sin(\frac{9\tau\omega_Q}{2}) - 6\tau\omega_Q S_1 \cos(\frac{9\tau\omega_Q}{2})] I_{z,2}$
$-x$	x	$-\frac{48\alpha\omega_Q}{\pi} S_1 \sin(\frac{9\tau\omega_Q}{2}) I_{y,1} - \frac{48\alpha\omega_Q}{\pi} S_1 \cos(\frac{9\tau\omega_Q}{2}) I_{y,2} + [C_1 \cos(\frac{9\tau\omega_Q}{2}) + 6\tau\omega_Q S_1 \sin(\frac{9\tau\omega_Q}{2})] I_{z,1} + [C_1 \sin(\frac{9\tau\omega_Q}{2}) - 6\tau\omega_Q S_1 \cos(\frac{9\tau\omega_Q}{2})] I_{z,2}$
$-x$	$-x$	$-\cos(3\tau\omega_Q)I_{z,1} - \sin(3\tau\omega_Q)I_{z,2}$
y	y	$-\cos(3\tau\omega_Q)I_{z,1} + \sin(3\tau\omega_Q)I_{z,2}$
y	$-y$	$-\frac{48\alpha\omega_Q}{\pi} S_1 sin(\frac{9\tau\omega_Q}{2}) I_{x,1} + \frac{48\alpha\omega_Q}{\pi} S_1 \cos(\frac{9\tau\omega_Q}{2}) I_{y,2} + [C_1 \cos(\frac{9\tau\omega_Q}{2}) + 6\tau\omega_Q S_1 \sin(\frac{9\tau\omega_Q}{2})] I_{z,1} - [C_1 \sin(\frac{9\tau\omega_Q}{2}) - 6\tau\omega_Q S_1 \cos(\frac{9\tau\omega_Q}{2})] I_{z,2}$
$-y$	y	$+\frac{48\alpha\omega_Q}{\pi} S_1 \sin(\frac{9\tau\omega_Q}{2}) I_{x,1} - \frac{48\alpha\omega_Q}{\pi} S_1 \cos(\frac{9\tau\omega_Q}{2}) I_{x,2} + [C_1 \cos(\frac{9\tau\omega_Q}{2}) + 6\tau\omega_Q S_1 \sin(\frac{9\tau\omega_Q}{2})] I_{z,1} - [C_1 \sin(\frac{9\tau\omega_Q}{2}) - 6\tau\omega_Q S_1 \cos(\frac{9\tau\omega_Q}{2})] I_{z,2}$
$-y$	$-y$	$-\cos(3\tau\omega_Q)I_{z,1} + \sin(3\tau\omega_Q)I_{z,2}$

$C_1 = \cosh[\frac{3}{2}\sqrt{-(\tau^2+\frac{64\alpha^2}{\pi^2})}\omega_Q]$, $S_1 = \sinh[\frac{3}{2}\sqrt{-(\tau^2+\frac{64\alpha^2}{\pi^2})}\omega_Q]$, ω_Q is the quadrupolar coupling constant, 2α is the $\pi/2$ pulse width and we have set $\frac{\gamma\hbar B_o}{kT} = 1$.

where $w_1 = \frac{12\alpha\omega_Q}{\pi}$ and $\omega = 6\tau\omega_Q$. The above expression indicates that the detected signal will have a finite pulse width contribution due to the presence of the coherence terms $I_{x,2}$ and $I_{y,2}$, which do not commute with the quadrupolar Hamiltonian and evolve to detectable signal, as shown previously. Consequently, this cycle does not exactly remove the finite pulse width contributions to the detected signal as did the phase cycle shown in Eq. (18), even though it is robust against suppressing spurious artifacts due to the electronic ringing of both pulses. The finite pulse width contribution multiplying the terms $I_{x,2}$ and $I_{y,2}$ for this cycle vary approximately inversely with τ, and depending on the strength of the quadrupolar interaction it is expected that long pulse spacings would still make this phase cycle robust against finite pulse width artifacts as well.

3. Simulation

To confirm the results of the calculations and illustrate the spectral distortion introduced by finite pulse width effects, we carried out a simulation of spin $I = 1$ nuclei subject to a strong magnetic field evolving under the first-order quadrupolar interaction and the RF pulse sequence shown in Fig. 1.

Given the density matrix of the spin system at the time 3τ from Table 3, the state of the system at any point in time t_k is given by

$$\rho(t_k) = \exp(-iH_Q t_k)\rho(3\tau)\exp(iH_Q t_k) \tag{24}$$

where H_Q is given in Eq. (1). The detected signal at time t_k is found from performing the computation

$$\text{Signal}(t_k) = \text{Trace}\{\rho(t_k)[I_{x,1} + iI_{y,1}]\} \tag{25}$$

The simulated spectra were developed by using a dwell time equal to 0.5 μs and a quadrupolar coupling constant equal to 125 kHz. We assumed a sample with a random distribution of orientations, a quadrupolar asymmetry parameter η=0, and varied the pulse width 2α over the range of 0.5–2 μs. The results are shown in Fig. 2 for a cycle where the first pulse was a $\pi/2$ about the x-axis, and the second pulse was a $\pi/2$ about the y-axis. The simulation illustrates that without phase cycling the spectra are dependent on the pulse width, and that the powder pattern becomes more asymmetric as the pulse width increases from 0.5 μs (Fig. 2A) to 2 μs (Fig. 2C). A similar pattern is observed

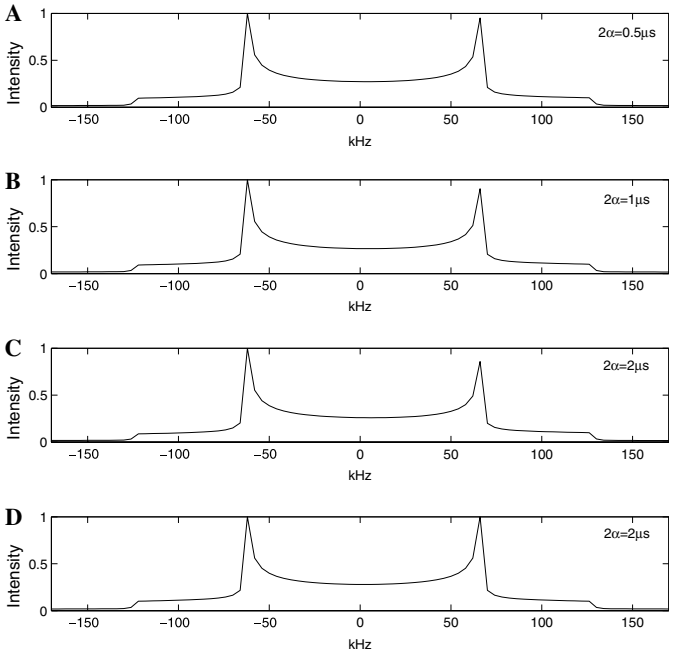

Fig. 2. Simulated quadrupolar echo spectra based on the two pulse sequence in Fig. 1, with a $\pi/2$ pulses about the x-axis followed by a $\pi/2$ pulse about the y-axis without any phase cycling. The figure highlights the spectral distortion introduced (asymmetric powder pattern) due to finite pulse widths of (A) 0.5 μs, (B) 1 μs and (C) 2 μs. (D) Simulated quadrupolar echo spectra based on the two pulse sequence in Fig. 1, for 2 μs pulses with the phase cycling scheme indicated in Eq. (18) of the text highlighting the finite pulse width artifact suppression.

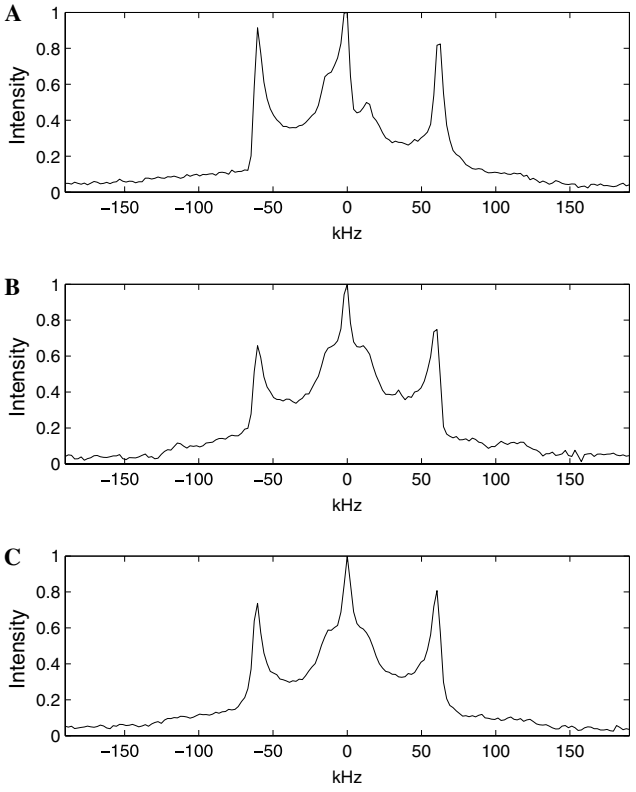

Fig. 3. (A) Normalized experimental quadrupolar echo spectra of deuterated polyethelene based on the two pulse sequence in Fig. 1 with a $\pi/2$ pulse about the x-axis followed by a $\pi/2$ pulse about the y-axis without any phase cycling. The figure highlights the spectral distortion introduced (asymmetric powder pattern) due to finite pulse widths in agreement with our simulated result shown in Fig. 2C. The peak in the middle of the powder pattern is due to a highly mobile group and has been observed by others in the same sample [15]. (B) Normalized experimental quadrupolar echo spectra acquired on the same sample based on the two pulse sequence in Fig. 1 and the phase cycling scheme given in Eq. (22) of the text. (C) Normalized experimental quadrupolar echo spectra based on the two pulse sequence in Fig. 1 and the phase cycling scheme given in Eq. (18), highlighting the robust finite pulse width artifact suppression. In all of the experiments $\tau = 40$ μs and $2\alpha = 2$ μs.

for all remaining seven cycles given in Table 3 as well as that of the phase cycling scheme developed by Furo and Hedin suggested in Eq. (21). Fig. 2D highlights the result when the signals are co-added using the phase cycling scheme suggested in Eq. (18), and the distortion is removed resulting in symmetric spectra.

4. Experimental results

We performed an experiment to verify these findings on a Varian Inova 500 MHz NMR spectrometer using a Doty model DSI 431 solid state NMR probe. A sample of powdered deuterated polyethelene was purchased from Polymer Source, Inc. located in Montreal, Canada. Our experimental procedure involved putting the nuclear spins on resonance and tuning the $\pi/2$ pulses and requisite RF power using a sample of deuterated water with well known tuning procedures used in solid state multiple pulse NMR [1]. In the experiments, the spacing of τ was set to 40 μs, the dwell time was set to 0.5 μs and 2416 scans were collected with a recycle delay of 5 s at room temperature.

Fig. 3A–C highlight the experimental data acquired with and without phase cycling schemes for a readily achievable 2 μs pulse width. The presence of the narrow line in the center of the powder pattern is due to highly mobile regions of the sample where the quadrupolar Hamiltonian is partially averaged away and has been observed by others in deuterated polyethelene [15]. For the purposes of our work, this feature can be disregarded. In Fig. 3A, the experimental data illustrate that without phase cycling the peaks of the quadrupolar powder pattern appear asymmetric as expected from our analysis and simulation. In contrast, Fig. 3C shows that when the phase cycling scheme given in Eq. (18) is implemented, the spectral distortion is removed and the horns of the quadrupolar powder pattern appear symmetric. We also tested the cycle suggested by Furo and Hedin [7] given in Eq. (22). Fig. 3B shows the spectra acquired with this cycle, highlighting a slight asymmetry in the quadrupolar powder pattern. With longer spacings between pulses, the spectral distortion with this cycle is less apparent.

Though our analysis has assumed that the $\pi/2$ pulses delivered to the spin system are perfect, this cannot be achieved in practice as the RF field strength varies spatially across the sample. In practice one should ensure that the sample is centered in the RF coil and a coil that produces a homogeneous field over the sample is used [21]. To further improve the efficiency of suppressing artifacts due to finite pulse widths, one aught to consider the higher order terms of the Magnus expansion. It is well known in solid state NMR that higher order terms of the Magnus expansion of this two pulse cycle for the dipolar Hamiltonian are not zero since the toggling frame Hamiltonians at different times do not commute with one another [1]. While the higher order terms of the Magnus expansion for this cycle have not been worked out for the quadrupolar Hamiltonian, the experimental results indicate that the first-order contribution of finite pulse widths to distorting the spectra is well suppressed with the suggested phase cycling scheme. With shorter pulse widths and higher RF power, it is expected that the distortion can be further reduced, and the features on the tail ends of the quadrupolar powder pattern can be better resolved.

5. Conclusions

Average Hamiltonian theory was applied for creating a phase cycling scheme that removes finite pulse width artifacts in the spectra of spin-1 nuclei acquired with the familiar two pulse echo experiment. Our results are verified both with a simulation tool written in Matlab and experimentally on a sample of deuterated polyethelene. It is expected that a similar analysis can be performed on composite pulse cycles or other pulse sequences where finite pulse widths may introduce similar spectral distortions.

Acknowledgments

We thank Professor S. Greenbaum of Hunter College for allowing us to use the Varian Inova NMR spectrometer in his laboratory, and Nicole Leifer and Ameesh Khalfan for assisting us in setting up the experiments. We also thank Gabor Borzsonyi of the University of Alberta, Dr. Nicolas Boulant of the Departement de Recherche sur l'Etat Condense, les Atomes et les Molecules and Rabia Roopchand of York College for useful discussions. E.S. Mananga acknowledges support by The City University of New York Graduate Center Alliances for Graduate Education in the Professoriate (AGEP) program funded by the National Science Foundation. Y.S. Rumala thanks the Department of Education McNair Scholars program as well as the National Science Foundation Louis Stokes Alliance for Minority Participation program for their support.

References

[1] B.C. Gerstein, C.R. Dybowski, Transient techniques in NMR of solids. An introduction to theory and practice, Academic Press, Orlando, 1985.
[2] M. Mehring, Principles of high resolution NMR in solids, Springer-Verlag, Berlin, 1983.
[3] H.W. Speiss, Molecular dynamics of solid polymers as revealed by deuteron NMR, Colloid Polym. Sci. 261 (1983) 193–209.
[4] D. Hentschel, H. Sillescu, H.W. Speiss, Deuteron n.m.r. study of chain motion in solid polyethylene, Polymer 25 (1984) 1078–1086.
[5] H.W. Speiss, NMR, Basic principles and progress, vol. 15, Springer-Verlag, Berlin, 1978.
[6] R.G. Griffin, Solid state NMR of lipid bilayers, Methods Enzymol. 72 (1981) 108–174.
[7] I. Furo, N. Hedin, Noise reduction in quadrupolar echo spectra at short echo times, J. Magn. Reson. 152 (2001) 214–216.
[8] A.D. Ronemus, R.L. Vold, R.R. Vold, Deuterium quadrupole echo NMR spectroscopy II. Artifact suppression, J. Magn. Reson. 70 (1986) 416–426.
[9] D. Suter, M.H. Levitt, R.R. Ernst, Composite pulse excitation in three-level systems, J. Chem. Phys. 8 (1984) 3064–3068.

[10] W.S. Warren, Effects of arbitrary laser or NMR pulse shapes on population inversion and coherence, J. Chem. Phys. 81 (1984) 5437–5448.
[11] Y. Millot, P.P. Man, Determination of quadrupole parameters with a composite pulse for spurious signal suppression, J. Magn. Reson. 150 (2001) 10–16.
[12] R. Fu, V.L. Ermakov, G. Bodenhausen, Divergent double chirp pulses for refocusing quadrupolar interactions, Solid State Nucl. Magn. Reson. 7 (1996) 1–10.
[13] P. Bilski, A.M. Panich, N.A. Sergeev, J. Wasicki, Simple two-pulse time-reversal sequence for dipolar and quadrupolar-coupled spin systems, Solid State Nucl. Magn. Reson. 25 (2004) 76–79.
[14] M. Bloom, J.H. Davis, M.I. Valic, Spectral distortion effects due to finite pulse widths in deuterium nuclear magnetic resonance spectroscopy, Can. J. Phys. 58 (1980) 1510–1517.
[15] P.M. Henrichs, J.M. Hewitt, M. Linder, Experimental aspects of deuterium NMR of solids, J. Magn. Reson. 60 (1984) 280–298.
[16] S. Vega, A. Pines, Operator formalism for double quantum NMR, J. Chem. Phys. 66 (1977) 5624–5644.
[17] U. Haeberlen, J.S. Waugh, Coherent averaging effects in magnetic resonance, Phys. Rev. 175 (1968) 453–467.
[18] A. Jerschow, From nuclear structure to the quadrupolar NMR interaction and high-resolution spectroscopy, Prog. Nucl. Magn. Reson. Spectrosc. 46 (2005) 63–78.
[19] D.I. Hoult, R.E. Richards, Critical factors in the design of sensitive high resolution nuclear magnetic resonance spectrometers, Proc. R. Soc. Lond. Series A 344 (1975) 311–340.
[20] S. Antonijevic, S. Wimperis, Refocussing of chemical and paramagnetic shift anisotropies in ^{2}H NMR using the quadrupolar echo-experiment, J. Magn. Res. 164 (2003) 343–350.
[21] S. Idziak, W. Haeberlen, Design and construction of a high homogeneity RF coil for solid state multiple pulse NMR, J. Magn. Res. 50 (1982) 281–288.